THE GEOLOGICAL SOCIETY OF AMERICA®

Profiling interactions between the Westerlies and Asian summer monsoons since 45 ka: Insights from biomarker, isotope, and numerical modeling studies in the Qaidam Basin

Mingqiu Hou[1], Guangsheng Zhuang[1,†], Junliang Ji[2], Shuyuan Xiang[2], Wenwen Kong[3], Xingqian Cui[4], Minghao Wu[1], and Michael Hren[5]

[1]*Department of Geology and Geophysics, Louisiana State University, Baton Rouge, Louisiana 70803, USA*

[2]*School of Earth Sciences, China University of Geosciences, Wuhan, 430074, China*

[3]*Department of Geography and Berkeley Atmospheric Sciences Center, University of California, Berkeley, California 94720, USA*

[4]*Department of Earth, Atmospheric and Planetary Sciences, Massachusetts Institute of Technology, Cambridge, Massachusetts 02139, USA*

[5]*Center for Integrative Geosciences, University of Connecticut, Storrs, Connecticut 06269, USA*

ABSTRACT

The Qaidam Basin marks a crucial boundary between the Westerlies and the Asian summer monsoons. Previous studies in the Qaidam Basin have advanced our knowledge of the paleoclimate over glacial to interglacial cycles. However, our understanding of the paleoclimatic sensitivity of the Qaidam Basin to the relative strength of these two climatic driving forces remains limited due to the lack of regional paleoclimatic reconstructions. The Qaidam Basin is proposed as a regional and global eolian dust source during the glacial periods, during which a cold, dry climate is associated with the equatorward shift of the jet stream. On the contrary, paleoshoreline records suggest that a highstand lake stage prevailed in late Marine Isotope Stage 3 (MIS 3) and lasted until 15 ka. To address this conundrum, we have applied an integrated approach to reconstructing the regional paleoclimatic history by combining compound-specific isotope analysis, lake temperature reconstruction, and numerical modeling. Our results show varying paleoclimate associated with the dynamic climate boundary since 45 ka: (1) a wet climate during late MIS 3, when the Asian summer monsoons are strengthened under high summer insolation and penetrate further into Central Asia; (2) a general cold, dry but wetter than at present climate in the Last Glacial Maximum (LGM), when the Asian summer monsoons retreat and the Westerlies become dominant; and (3) three short periods of extreme aridity corresponding to the Younger Dryas and Heinrich 2 and 4 events, when the normal moisture transport via the Westerlies and Asian summer monsoons is interrupted. The numerical modeling supports an increase in the effective precipitation during the LGM due to reduced evaporation under low summer insolation. These results suggest that the Westerlies and Asian summer monsoons alternately controlled the climate in the Qaidam Basin in response to precessional forcing during the late Pleistocene.

INTRODUCTION

The Westerlies and the Asian summer monsoons played essential roles in controlling the paleoclimate of Central Asia. The Qaidam Basin is situated in a critical climatic region that separates arid, Westerly-influenced Central Asia to the west and summer monsoon-controlled East Asia to the east (Fig. 1). As one of the world's highest and driest places with extremely high ratios of evaporation (>3000 mm) versus precipitation (<180–220 mm) (Tian et al., 2001; Yao et al., 2013), the Qaidam Basin potentially contributes a significant amount of eolian dust transported by the Westerlies to the downwind areas of the Chinese Loess Plateau (Kapp et al., 2011; Pullen et al., 2011; Lin et al., 2020) and the North Pacific (Li et al., 2011a). The unique geographical location of the Qaidam Basin makes its hydrological changes sensitive to the relative strength of the Westerlies and Asian summer monsoons. However, the interactions between the two climate systems and their influence on eolian dust production in the Qaidam Basin at orbital and millennial scales are not well understood.

Paleoclimate in Central Asia was thought to have alternated between warm, humid interglacial periods strongly influenced by the Asian summer monsoons and cold, dry glacial periods dominantly influenced by the Westerlies (An et al., 2012). This alternating climate pattern has been manifested by the loess/paleosol sedimentary sequences from Tianshan in Central Asia (Li et al., 2016) and the Chinese Loess Plateau in East Asia (Kukla and An, 1989; An et al., 1990; Porter and An, 1995). In the Qaidam Basin, sedimentary records and modeling studies reveal that the cold, dry climate during the glacial and stadial periods resulted in subaerial exposure and intensive erosion of lacustrine strata when the main axis of the Westerly jet shifted toward the equator (Kapp et al., 2011; Pullen et al., 2011; Heermance et al., 2013; Rohrmann et al., 2013). High eolian fluxes recorded in sedimentary successions ranging from Central Asia to the North Pacific indicate strong wind erosion associated with Westerlies (Hovan et al., 1991; An et al., 2012; Li et al., 2016). Isotope proxy and pollen studies from the northern Tibetan Plateau suggest that precipitation decreased during the Last Glacial Maximum (LGM) (Wang et al., 2014; Thomas et al., 2016).

Paleoshoreline records from the Qaidam Basin, particularly freshwater mollusks in lacustrine strata, indicate the expansion of paleo-lakes from ca. 30–40 ka to ca. 15 ka (Li and Zhu, 2001; Zhang et al., 2008). This lake expansion coincides with the interglacial temperature conditions during late Marine Isotope Stage 3 (MIS 3), which is supported by the Guliya ice-core $\delta^{18}O$

Guangsheng Zhuang http://orcid.org/0000-0002-7024-1446

†Corresponding author: gzhuang@lsu.edu.

GSA Bulletin; https://doi.org/10.1130/B35751.1; 6 figures; 1 supplemental file.

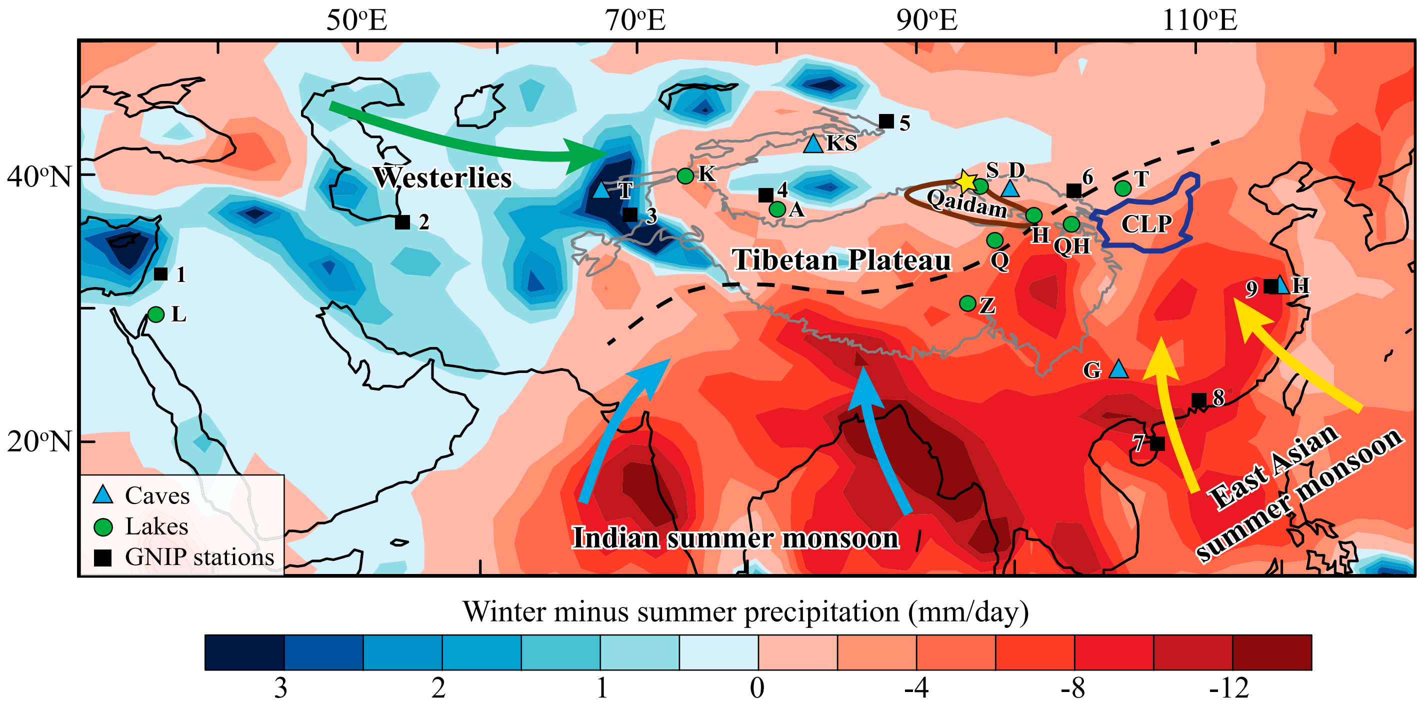

Figure 1. Thirty-year (1981–2010) record of winter (December–January–February) minus summer (June–July–August) precipitation (mm/day) is shown. Blue represents greater precipitation in winter (December–January–February), while red indicates greater precipitation in summer (June–July–August). Data are derived from the National Centers for Environmental Prediction. Reanalysis provided by National Oceanic and Atmospheric Administration Earth System Research Laboratories Physical Science Division at Boulder, Colorado, USA (https://www.esrl.noaa.gov/psd/data). The gray line outlines the 3000 m contour on the Tibetan Plateau and surrounding mountain (adapted from Li et al., 2019). The Qaidam Basin (brown outline), core site (yellow star), and the Chinese Loess Plateau (CLP; dark blue outline) are noted. Arrows highlight the moisture transport via the Westerlies (green), Indian summer monsoons (blue), and East Asian summer monsoons (yellow). The black, dashed line represents the modern boundary between the Asian summer monsoons (East Asian and Indian summer monsoons) and the Westerlies. Blue triangles are the locations of isotope reconstruction of paleometeoric waters in the Hulu (H) (Wang et al., 2008), Dongge (G) (Dykoski et al., 2005), Ton (T), and Kesang (KS) (Cheng et al., 2012) Caves and the Dunde Ice core (D) (Thompson et al., 1989). Green circles denote the lakes and paleo lakes discussed in the text: Lake Qinghai (QH) (Hou et al., 2016), Lake Sugan (S) (He et al., 2013; Wang et al., 2013), Lake Keluke (H) (Rao et al., 2014), Tengger Desert (T), Qarhan (Q), Zabuye (Z), Aksayqin (A) (Yu et al., 2003), Karakul (K) (Aichner et al., 2019), and Lisan (L) (Bartov et al., 2003). Black squares indicate the Global Network of Isotope in Precipitation (GNIP) meteorological stations (IAEA/WMO, 2006). Numbers are correlated with stations in Fig. S1 (see footnote 1).

record and the pollen record from the adjacent Qilian Shan (Thompson et al., 1997; Herzschuh et al., 2006). There are disparate interpretations of the highstand or lake expansion through late MIS 3. One interpretation invokes the inland penetration of Asian summer monsoons (Shi et al., 2001). The other attributes the increase of precipitation during late MIS 3 to the strong circulation of the Westerlies (Yang et al., 2004).

Previous studies using geochemical, biomarker, and isotopic proxies and numerical simulations have provided insight into the variations of the Westerlies and the Asian summer monsoons and their influences on the paleohydrology, but most studies focus on either the core area of the Westerlies further west (e.g., speleothem from Kesang Cave and Ton Cave in the Tian Shan and lacustrine records from the Lake Karakul in Pamirs, Fig. 1) (Cheng et al., 2016; Aichner et al., 2019) or the Asian summer monsoon-influenced regions to the east (e.g., lacustrine records from Lake Qinghai) (An et al., 2012; Thomas et al., 2016). Despite active research that has reconstructed paleoclimatic evolution in the northern Tibetan Plateau during the Holocene (An et al., 2012; Thomas et al., 2016), studies of past climate in the Qaidam Basin on orbital timescales (e.g., precession cycles) are not available. In this study, we aim to resolve how and at what timescale the paleoclimate in the Qaidam Basin responded to the relative strength of the Westerlies and the Asian summer monsoons. We focus on three related questions: (1) does the high summer insolation period (corresponding to MIS 3) cause strong summer monsoons with high temperatures and increased precipitation? (2) Does the transition from high to low summer insolation into the LGM weaken the summer monsoons? (3) Is evaporation reduced during the LGM relative to at present? To answer these questions, we conduct an integrated study using organic biomarker-proxies coupled with climate modeling to examine the paleoclimatic history of the Qaidam Basin during the last glacial period. We apply hydrogen isotopic analysis to terrestrial higher-plant *n*-alkanes and apply the locally calibrated alkenone-based paleothermometry (U^{K}_{37}) to lacustrine sediments recovered from a drill core in the western Qaidam Basin. Reconstructed paleoclimatic history, along with numerical modeling studies using the Community Earth System Model (CESM) version 1.3, are compared with the Holocene regional paleoclimatic proxy records in the Asian summer monsoon- and Westerly-dominated areas.

GEOLOGICAL SETTING AND MODERN CLIMATE

The Qaidam Basin is an intermontane basin at the northern margin of the Tibetan Plateau. It

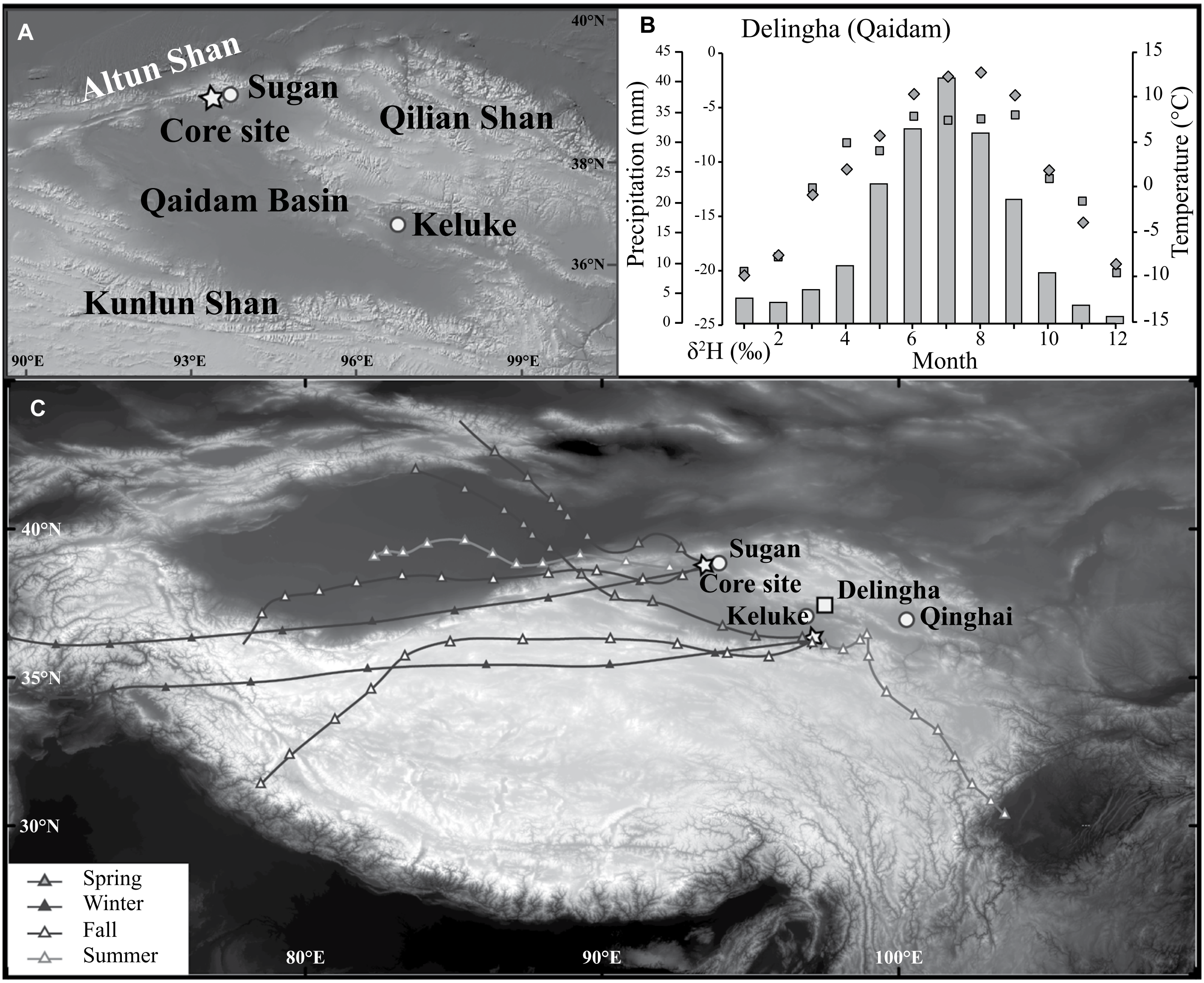

Figure 2. (A) Topographic map of the northern Tibetan Plateau shows the coring site (star, this study) in the Qaidam Basin and locations of Lake Sugan (Wang et al., 2013) and Lake Keluke (Rao et al., 2014) discussed in the text. (B) Meteorological data from the Tibetan Network of Isotopes in Precipitation (TNIP) at the Delingha station (monthly mean precipitation amount, column; monthly mean temperature, diamond; monthly mean hydrogen isotope (δ^2H) values of precipitation, square) (Yao et al., 2013). (C) HYbrid Single-Particle Lagrangian Integrated Trajectory Model (HYSPLIT) trajectories for summer, fall, winter, and spring air masses 72 h before the arrival at the core site and a site (black star) in the eastern Qaidam Basin. The HYSPLIT model is based on National Centers for Environmental Prediction reanalysis data from 2018 to 2019 (https://www.arl.noaa.gov/hysplit). The TNIP station in Delingha (square) and lakes (circles) in the northern Tibetan Plateau discussed in the text are noted.

is bounded by the Qilian Shan fold-thrust belt to the northeast, the Altun Shan range to the northwest, and the East Kunlun Shan range to the south (Fig. 2A). The Qaidam Basin is ca. 700 km in length with a maximum width of ~300 km and occupies ~120,000 km^2 with a mean elevation of 2700 m (Chen and Bowler, 1986). The geomorphology of the Qaidam Basin is characterized by widespread eolian features including migrating dunes, deflecting pans, and mega-yardangs due to extremely arid climate and severe wind erosion (Goudie, 2007). The lake system in the modern Qaidam Basin comprises more than 20 discrete salt lakes and playas and occupies a quarter of the total basin area (Chen and Bowler, 1986).

In the Qaidam Basin, more than 90% of the annual rainfall occurs during the spring and summer seasons (Tian et al., 2001); the average temperatures for January and July and the mean annual temperature are −12 °C, 16 °C, and 2 °C, respectively (Zhang et al., 2008) (Fig. 2B). Water vapor is transported mainly by the Westerlies with a substantial amount coming from local recycling (Bershaw et al., 2012; Li and Garzione, 2017); moisture from the Asian summer monsoons reaches the eastern part of the basin (Araguás-Araguás et al., 1998; Tian et al., 2001; Yao et al., 2012; Caves et al., 2015). We used the HYbrid Single-Particle Lagrangian Integrated Trajectory Model (HYSPLIT) to track the air masses of the study area in the western Qaidam Basin and those at a site selected in the eastern Qaidam Basin. The air

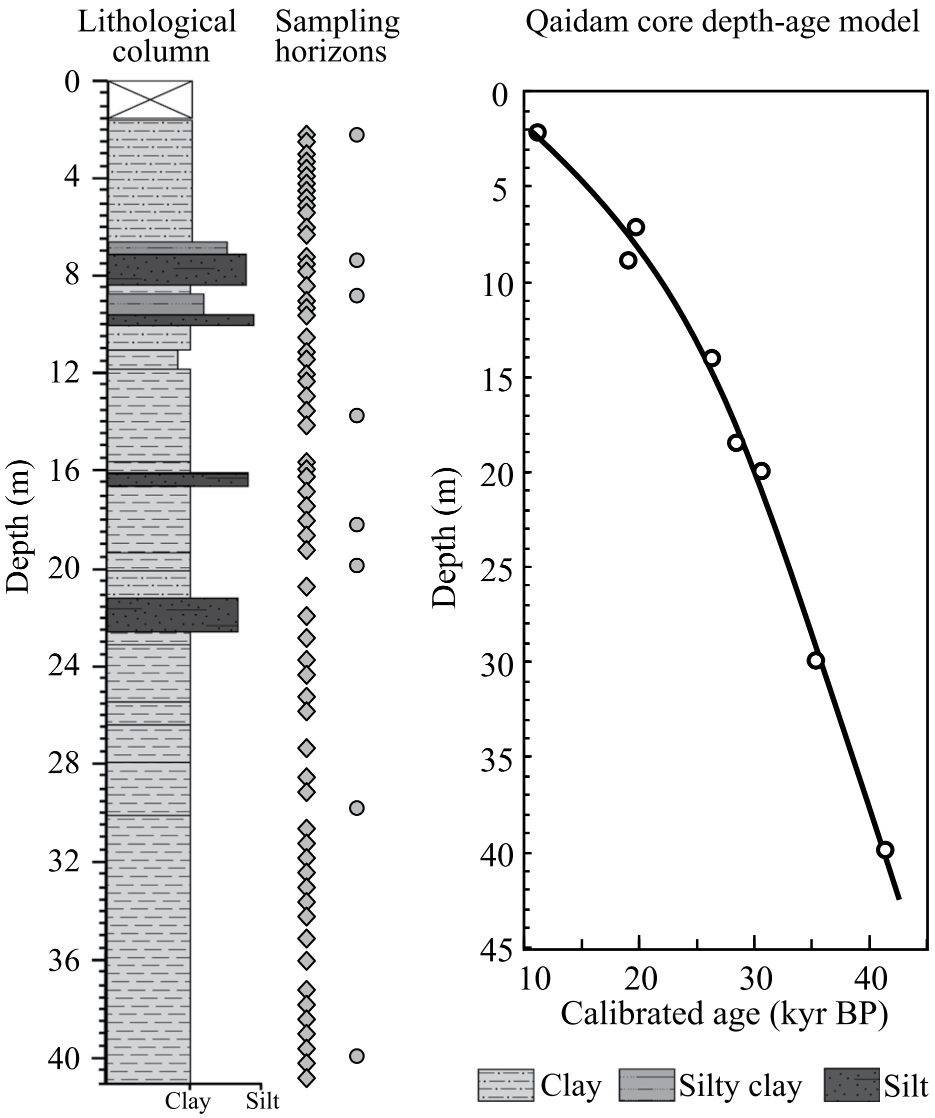

Figure 3. The lithostratigraphic column and the chronology of the core in the western Qaidam Basin are shown. The age model is constructed by applying the third order polynomial correlation of eight radiocarbon ages with the corresponding depth. Samples are analyzed for leaf wax hydrogen isotopes and U^{K}_{37} temperatures (diamonds) and ^{14}C ages (circles).

masses modeled indicate that the eastern Qaidam Basin receives moisture from Asian summer monsoons during summer and from the Westerlies in other seasons. The western Qaidam Basin is influenced by Westerlies year-round (Fig. 2C).

MATERIALS AND METHODS

Sediment samples were obtained from a 42-m-long core in the western Qaidam Basin (38° 4′N, 93° 0′E, 2754 m above sea level; Figs. 1 and 2). The core, which is composed of late Pleistocene lacustrine sediments, is overlain by Holocene evaporites. Sediments primarily consist of unconsolidated clay and silt with sparse interbedded gypsum and halite. We reconstructed the paleohydrology of the Qaidam Basin by studying the compound-specific hydrogen isotopes of long-chain *n*-alkanes ($\delta^2H_{n\text{-alk}}$) with 29 and 31 carbon atoms (*n*-C29 and *n*-C31) derived from terrestrial higher plants (Eglinton and Hamilton, 1967). $\delta^2H_{n\text{-alk}}$ reflects the change in precipitation δ^2H and has been increasingly used in paleohydrology studies (Sachse et al., 2012). We compare the new isotopic data with the Holocene records from Lake Keluke (Rao et al., 2014) and Lake Sugan (Wang et al., 2013) in the same basin to understand the temporal and spatial variations of climate. The relative input of aquatic versus terrestrial organic material is evaluated by the biomarker proxy P_{aq} (Ficken et al., 2000) that provides ancillary information on the depositional facies associated with expansion and contraction of lake volume. Lake surface temperatures are reconstructed by the alkenone-unsaturation index (U^{K}_{37}) (Brassell et al., 1986; Prahl and Wakeham, 1987; Schouten et al., 2002)—a temperature proxy that has been used for estimating temperature variations of Lake Qinghai during the Holocene (Hou et al., 2016). The CESM 1.3 climate models are used to examine the differences between the pre-industrial period and the LGM in precipitation, evaporation, and surface runoff during summer, in which the major rainfall occurs.

Radiocarbon Dating

Eight fine-grained clays were selected at specific depths and analyzed for ^{14}C ages (Fig. 3). Bulk sediments were analyzed for ^{14}C ages by accelerator mass spectrometry (AMS) at Beta Analytic Testing Laboratory. Sediments were grounded and sieved to <180 microns and then treated with HCl acid to remove inorganic carbon prior to analysis. A major issue in radiocarbon dating is the reservoir effect that introduces inherited age and residence age (Hendy and Hall, 2006). The inherited age can derive from the input of old carbon by river water that carries dissolved carbonate from the drainage system, while the residence age is caused by a delay in CO_2 exchange rates between the atmosphere and lake bottom water. A review paper on the reservoir effect on the Tibetan Plateau reveals that reservoir ages vary spatially and temporally over the Tibetan Plateau (Hou et al., 2012). The standard approach for deriving the reservoir age is to compare the ^{14}C ages of modern in situ carbon (e.g., extant plant materials and organic matter of surface sediments) and/or the coexistent plant remains with measured ^{14}C ages. The overlying Holocene succession in the core site is eroded due to subaerial exposure, and thus the reservoir age cannot be obtained with modern lake surface sediments. Hence, we used the reservoir age derived from adjacent Lake Sugan in western Qaidam Basin (Fig. 1) to calibrate our sample ages. The reservoir age of Lake Sugan is estimated to be 2627 years based on the age difference between varve-based ages and those of coexisting plants (Zhou et al., 2009). The varve-based ages are determined by the number of dark and light laminae couplets that characterize the seasonal variation of limnological conditions (Zhou et al., 2007). We subtract the reservoir age from the measured ^{14}C ages to derive the reservoir-corrected ^{14}C ages that are subsequently calibrated by Calib 7.0.4 software (Fig. 3).

Lipid Extraction

Total lipids were extracted with a Soxhlet extractor using the azeotrope of dichloromethane/

methanol (DCM/MeOH; 2:1 v/v) for 48 h. The lipid extracts were evaporated under a stream of pure nitrogen until dry. Organic compounds in total lipid extracts were separated into apolar, intermediate, and polar fractions using a pipette column filled with ca. 0.5 g of activated silica gel and eluted with 2 ml hexane, 4 ml DCM, and 4 ml methanol sequentially.

n-Alkanes contained in the apolar fractions were re-dissolved into 1500 µL of hexane, and *n*-alkane abundances were determined using a Thermal Trace 1310 Gas chromatography (GC)-flame ionization detector (FID) fitted with a programmable temperature vaporization (PTV) injector and TG-1MS column (60 m long, 0.25 mm i.d., 0.25 µm film thickness). Samples were carried by helium at a rate of 2 ml/min. GC oven temperature is ramped from 60 °C (holding for 1 min) to 320 °C at a rate of 15 °C/min (holding for 20 min). Individual *n*-alkanes were identified by comparing the elution time with a reference standard (Mix A6, Schimmelmann, Indiana University Bloomington).

The carbon preference index (CPI) of *n*-alkanes is determined using the equation:

$$CPI = \frac{1}{2}\frac{\sum A(23+25+27+29+31+33) + \sum A(25+27+29+31+33+35)}{\sum A(24+26+28+30+32+34)} \quad (1)$$

where A stands for the areas of the individual *n*-alkanes that are estimated by using the software Xcalibur for chromatography analysis. The numbers 23–35 represent the chain length of *n*-alkanes.

The *n*-alkane distributions of terrestrial higher plants are maximized at n-C_{29} and n-C_{31}, while submerged/floating plants are predominated by n-C_{23} and n-C_{25}. P_{aq} index is defined by the relative proportion of mid-chain (n-C_{23} and n-C_{25}) to long-chain *n*-alkane (n-C_{29} and n-C_{31}) homologs (Ficken et al., 2000):

$$P_{aq} = \frac{A(23+25)}{A(23+25+29+31)} \quad (2)$$

where A is identical to that in the equation for CPI, and the numbers indicate the chain length of odd-numbered *n*-alkanes.

Compound-Specific Hydrogen Isotope Analysis

Compound-specific hydrogen isotopes were measured using a Trace Gas chromatography (GC) 1310 coupled to a Thermo Delta V Advantage isotope ratio mass spectrometer (IRMS) interfaced with a Thermo Isolink interface. The GC column and carrier gas flow rate were identical to the GC-FID conditions. Compounds were separated on the GC with the temperature being programmed from 60 °C (held for 1 min) to 170 °C at 14 °C/min, to 300 °C at 3 °C/min, and then to 325 °C at 14 °C/min with an isothermal holding of 10 min. H_3^+ factor was measured daily prior to isotopic analysis with an average of 8.5 ppm (n = 3). Samples were analyzed in duplicate with a mean analytical precision of 1.5‰. Hydrogen isotope ratio values were determined relative to the reference gas, calibrated against Mix A6 (n-C_{16} to n-C_{30}; Arndt Schimmelmann, Indiana University), and reported relative to VSMOW with two standard errors using the equation:

$$\delta^2 H = \left(\frac{R_{sample}}{R_{standard}} - 1\right) \times 1000 \quad (3)$$

where R stands for the $^2H/H$ ratios of samples and reference materials. The $\delta^2H_{n\text{-alk}}$ values are reported to Vienna Standard Mean Ocean Water (VSMOW) and expressed in per mil (‰).

We focus discussions on the weighted mean $\delta^2H_{n\text{-alk}}$ values of n-C_{29} and n-C_{31}, which are calculated using the equation:

$$\delta^2 H_{n\text{-alk}} = \frac{\sum A_i \times \delta^2 H_i}{\sum A_i} \quad (4)$$

where A stands for the areas of individual *n*-alkanes, and *i* (29 and 31) indicates carbon chain lengths.

Alkenone Analysis

The solvent fraction containing alkenones was analyzed on a Thermal Trace 1310 Gas chromatography (GC)-flame ionization detector (FID) fitted with programmable temperature vaporization (PTV) injector using a TG-1MS column (60 m long, 0.25 mm i.d., 0.25 µm film thickness) and a helium flow rate of 2 ml/min. The GC oven temperature was ramped from 60 °C (holding for 1 min) to 280 °C at 20 °C/min and then to 325 °C at 2 °C/min with isothermal holding for 25 min. $C_{37:4}$, $C_{37:3}$, and $C_{37:2}$ methyl alkenones display typical peak clusters that can be identified by the identical retention time to the internal laboratory reference sample on GC-FID. Typical samples were analyzed on Gas chromatography-mass spectrometry (GC-MS) at the Massachusetts Institute of Technology to confirm the identification of alkenones. On GC-MS, alkenones are identified by the major ion fragment of m/z 81 and molecular ions of m/z 530.5, 528.5, and 526.5 for $C_{37:2}$, $C_{37:3}$, and $C_{37:4}$, respectively. The GC retention time and mass spectrum of the representative sample (ZK1405-3-4) are shown in Fig. S2[1]. Relative abundances of $C_{37:4}$, $C_{37:3}$, and $C_{37:2}$ alkenones were calculated using integrated areas determined through the Xcalibur software. Alkenone unsaturation indices (U_{37}^K) were determined by the equation (Prahl and Wakeham, 1987):

$$U_{37}^K = \frac{C_{37:2} - C_{37:4}}{C_{37:2} + C_{37:3} + C_{37:4}} \quad (5)$$

The conversion of U_{37}^K to temperature is based on calibration using modern lake surface sediments in the Tibetan Plateau that construct a relationship between U_{37}^K and summer lake surface temperature (Wang and Liu, 2013; Hou et al., 2016):

$$T = 17.571 \times U_{37}^K + 20.849 \quad (R^2 = 0.8059, n = 26) \quad (6)$$

We apply this relationship to convert our U_{37}^K data to lake temperature.

Climate Simulation during the LGM

We use the Community Earth System Model (CESM) version 1.3 to examine changes in precipitation, evaporation, runoff, and effective precipitation during the LGM relative to pre-industrial (PI) levels in summer. Effective precipitation is expressed as the following equation:

$$P_e = P_t - E - R \quad (7)$$

where P_e represents effective precipitation, which equals total precipitation (P_t) minus evaporation (E) and runoff (R) (Oleson et al., 2010). Models include the coupler and active atmosphere, land, ocean, and ice components. We examine two fully coupled experiments, each representing the simulated climate in the PI and the LGM, to further test changes in precipitation, evaporation, runoff, and effective precipitation during the summer of the LGM (21 ka) relative to the PI. The PI simulation is performed by Zhu et al. (2017), and all climatic forcing for the PI is fixed at values from A.D. 1850. The LGM is an extension of the simulation in Zhu et al. (2017), and the results of this extended LGM experiment were recently reported in (Tierney et al., 2020). Boundary conditions of the LGM,

[1]Supplemental Material. Figures S1–S2 and Tables S1–S3. Please visit https://doi.org/10.1130/GSAB.S.13180184 to access the supplemental material, and contact editing@geosociety.org with any questions.

including greenhouse gases (GHGs), orbital parameters, and ice sheets, follow the PMIP4 protocol (Kageyama et al., 2017). Specifically, CO_2, CH_4, and N_2O are set to 190 ppm, 375 ppb, and 200 ppb in simulations, respectively. The ICE-6G reconstruction 6G (Peltier et al., 2015) is used for the ice sheet, and the associated changes in surface elevation, albedo, and land-ocean distribution are derived from the ICE-6G reconstruction. This LGM simulation well captures the global cooling estimated from proxy data synthesis (Tierney et al., 2020).

RESULTS AND DISCUSSIONS

^{14}C Ages of the Qaidam Core

We obtained eight radiocarbon ages from bulk sediments. The chronology of eight radiocarbon dating ages is best modeled with the third order polynomial curve that is extrapolated to derive the youngest (ZK1405-2-1; 10,878 yr) and oldest (ZK1405-44-24; 45,648 yr) ages. Ages for samples between dating points are derived from interpolation. The established chronology enables us to interpret biomarker and isotope proxy records on the millennial time scale.

Lake Temperature Reconstructions

The evolution trend of lake temperatures (Fig. 4A) broadly follows the Northern Hemisphere summer insolation, with high (low) temperatures corresponding to high (low) summer insolation (Fig. 4C). The lake temperatures are warm at 45–39 ka and 37–33 ka (Fig. 4A) similar to the temperatures in Lake Qinghai during the early Holocene (9–5 ka) and late Holocene (since ca. 3 ka) (Hou et al., 2016). Our lake temperature reconstructions agree with the pollen records of Qilian Shan that suggest an interglacial temperature condition with a higher tree line during the MIS 3 (Herzschuh et al., 2006). Low temperatures during 39–37 ka coincide with the Heinrich 4 (H4) event that occurs at ca. 38 ka in the Greenland ice core record (Hemming, 2004). The lake temperatures decrease and reach the second low stage during 21–19 ka, which is within the duration of global LGM (26.5–18 ka) (Mix et al., 2001; Clark et al., 2009); the average lake temperature is lower than the early Holocene Climate Optimum (9–5 ka) by >6 °C (Fig. 4A). Lake temperatures increase after the LGM, which is synchronous with Northern Hemisphere warming (Shakun et al., 2012) and interrupted by another significant cooling during the Younger Dryas (YD) at ca. 13 ka (Alley, 2000).

Distribution of *n*-Alkanes

The *n*-alkanes (from *n*-C_{23} to *n*-C_{35}) preserved within the sediment core have CPI values ranging from 1 to 12.8 with a mean of ~3.7 (Table S1; see footnote 1), indicating the least possibility of thermal alteration after deposition (Eglinton and Hamilton, 1967). In addition, sediments have never been significantly buried or heated. The P_{aq} values—the proxy measuring the inputs of submerged/floating aquatic macrophytes relative to emergent and terrestrial species (Ficken et al., 2000)—vary from 0.05 to 0.63 with a mean value of ~0.39.

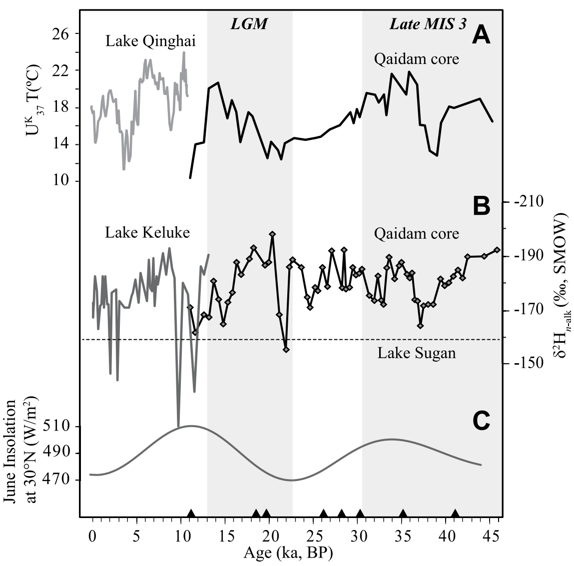

Figure 4. U^K_{37} temperatures and $\delta^2H_{n\text{-alk}}$ records since 45 ka are noted. (A) The alkenone-based U^K_{37} temperature records for the core between ca. 45 ka and 11 ka (black line; this study) and Lake Qinghai in the Holocene (gray line; Hou et al., 2016). (B) The weighted mean *n*-alkane hydrogen ($\delta^2H_{n\text{-alk}}$) isotope records of *n*-C_{29} and *n*-C_{31} from the core (diamonds; this study); $\delta^2H_{n\text{-alk}}$ record from Lake Keluke during the Holocene (gray line; Rao et al., 2014). The dashed line represents the mean $\delta^2H_{n\text{-alk}}$ value from a 1700-year-long record of $\delta^2H_{n\text{-alk}}$ for Lake Sugan (Wang et al., 2013). (C) June insolation at 30°N (Berger, 1978). Shaded bars show the intervals of the Last Glacial Maximum (LGM) and late Marine Isotope Stage (MIS) 3. Black triangles along the horizontal axis represent ^{14}C ages used for the age model of the Qaidam core.

Paleohydrology Reconstructions

$\delta^2H_{n\text{-alk}}$ values during the last glacial period are generally lower than the late Holocene values from Lake Sugan (Wang et al., 2013) except for three excursions with high isotopic values (Fig. 4B). The $\delta^2H_{n\text{-alk}}$ values vary between −181‰ and −199‰ at 45–39 ka followed by a positive shift with the highest value of −167‰ at 37 ka. After the excursion, the $\delta^2H_{n\text{-alk}}$ values shift to a low value of −192‰ at 35 ka. The low $\delta^2H_{n\text{-alk}}$ values persist until the second excursion occurs at 22 ka with the highest $\delta^2H_{n\text{-alk}}$ value of the whole time series: −152‰. The $\delta^2H_{n\text{-alk}}$ values shift from −152‰ at 22 ka to −204‰ at 20 ka and gradually increase until the end of the last glacial period.

Removal of Temperature Effect from $\delta^2H_{n\text{-alk}}$

The variation of modern precipitation δ^2H values in arid central Asia, including the Qaidam Basin, is driven predominantly by temperature (Araguás-Araguás et al., 1998) (Fig. 1 and S1; see footnote 1). Colder regional temperatures result in ^{2}H-depleted precipitations (hence low δ^2H values) due to the larger isotopic fractionation effect. However, low $\delta^2H_{n\text{-alk}}$ values during MIS 3 and deglaciation are unlikely to be the result of high lake temperatures as indicated by the U^K_{37} record (Fig. 4A). To investigate the effects of non-thermal factors on hydrogen isotopic composition, we first removed the effect of temperature on the $\delta^2H_{n\text{-alk}}$ record by subtracting the ^{2}H depletion and enrichment induced by temperature variations. The adjusted $\delta^2H_{n\text{-alk}}$ values are represented by $\delta^2H_{n\text{-alk-T}}$, reflecting the change of moisture source and water balance due to precipitation and evaporation. To reasonably compare hydrological conditions during the last glacial period and the Holocene, we use the same strategy to remove the temperature effect from the Holocene $\delta^2H_{n\text{-alk}}$ record for Lake Keluke (also called Lake Hurleg) in the eastern Qaidam Basin (Fig. 4B). The late Holocene alkenone-based U^K_{37} temperatures from Lake Qinghai (Hou et al., 2016) are considered feasible for inferring the contemporary temperature in the Qaidam Basin, as the annual temperatures of Lake Qinghai (0.1 °C) (An et al., 2012) are close to those of the Qaidam Basin (2 °C) at present (Yao et al., 2013). The detailed procedures for removing the temperature effect are as follows:

(1) We calculate the temperature differences (ΔT) for samples of the Qaidam Basin during the

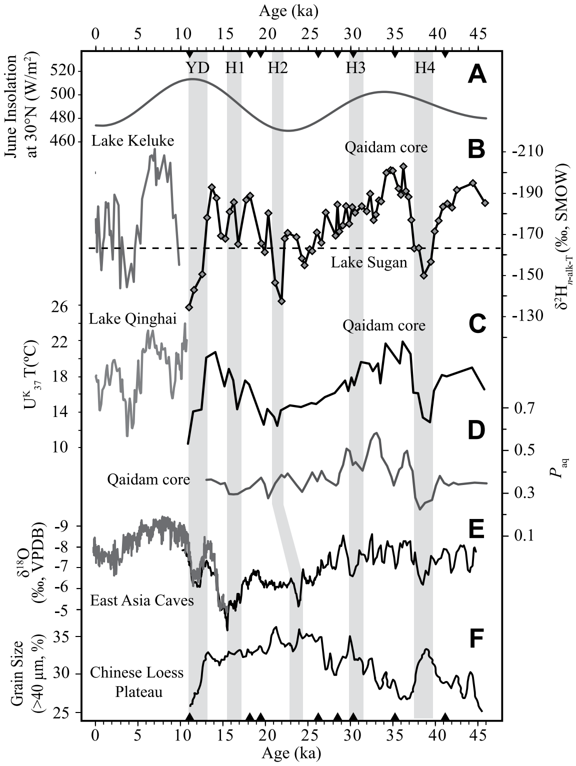

Figure 5. Regional paleoclimatic records since 45 ka are shown. (A) The insolation at 30°N in June (Berger, 1978). (B) Calculated $\delta^2H_{n\text{-alk-T}}$ values corrected for temperature effect on precipitation δ^2H for core samples in the western Qaidam Basin (diamonds; this study) and Lake Keluke in the eastern Qaidam Basin (gray line) (Rao et al., 2014). The dashed line represents mean $\delta^2H_{n\text{-alk-T}}$ values from Lake Sugan (Wang et al., 2013). (C) The U^K_{37}-based temperatures for the core (black line; this study) between 45 ka and 11 ka and Lake Qinghai in the Holocene (gray line; Hou et al., 2016). (D) Submerged aquatic macrophyte versus terrestrial higher plants (P_{aq}) ratio for the study core. (E) Speleothem $\delta^{18}O$ records from the Dongge (gray line; Dykoski et al., 2005) and Hulu Caves (black line; Wang et al., 2008). (F) Grain-size data from eolian deposits on the Chinese Loess Plateau (Rao et al., 2013). Gray bars denote the Younger Dryas (YD) and Heinrich events (H1 to H4). VPDB—Vienna Pee Dee Belemnite; SMOW—Standard Mean Ocean Water.

last glacial period relative to the latest Holocene temperature (18 °C) of Lake Qinghai (Hou et al., 2016).

(2) The δ^2H_p-$\delta^{18}O$ relationship from the meteorological station at Delingha is used to obtain the δ^2H_p temperature relationship. The slope of the $\delta^{18}O$ temperature relationship is 0.65‰/°C, and the slope of the local meteoric water line is 6.8 (Tian et al., 2003). The calculated slope of the δ^2H_p-temperature is 4.4‰/°C. The ΔT calculated in step (1) is then converted to the difference in δ^2H_p.

(3) The relationship between δ^2H_p and $\delta^2H_{n\text{-alk}}$ is expressed by the equation: $\varepsilon_{n-\text{alk/p}} = \delta^2H_{n-\text{alk}} + 1 / \delta^2H_p + 1 - 1. \varepsilon_{n-\text{alk/p}}$ is defined as the apparent fractionation factor (Polissar et al., 2009). Regional compilations of apparent fractionation across the Tibetan Plateau show that $\varepsilon_{n-\text{alk/p}}$ is invariant despite significant changes in climate and ecology across the plateau (Zhuang et al., 2014; Zhang et al., 2017). We use the $\varepsilon_{n-\text{alk/p}}$ values of −102‰ in the Qaidam Basin (Zhuang et al., 2014) to convert the temperature-dependent difference in δ^2H_p ($\Delta\delta^2H_p$) to that difference in $\delta^2H_{n\text{-alk}}$ ($\Delta\delta^2H_{n\text{-alk}}$).

(4) We correct $\delta^2H_{n\text{-alk}}$ by subtracting $\Delta\delta^2H_{n\text{-alk}}$ to obtain a $\delta^2H_{n\text{-alk}}$ record with the temperature effect removed ($\delta^2H_{n\text{-alk-T}}$).

(5) For comparison, we process the $\delta^2H_{n\text{-alk}}$ record of Lake Keluke and Lake Sugan in the same way (Fig. 5B).

The temperature-corrected $\delta^2H_{n\text{-alk-T}}$ record of the Qaidam core shows the larger amplitude and different structure of the isotope pattern as compared to those of the uncorrected $\delta^2H_{n\text{-alk}}$ record. This suggests there is a strong temperature control on terrestrial biomarker $\delta^2H_{n\text{-alk}}$ values in this area. The removal of temperature effect shifts $\delta^2H_{n\text{-alk-T}}$ values to more negative values between 30 ka and 37 ka with a minimum value of −203‰ while producing more positive values between 11 ka and 30 ka with a maximum value of −135‰ (Fig. 5B). After removing the temperature effect, our discussions focus on the temperature-corrected $\delta^2H_{n\text{-alk-T}}$ records to understand the evolution of the moisture source and precipitation/evaporation balance.

$\delta^2H_{n\text{-alk-T}}$ values vary in a wide range of ~70‰, reflecting dramatic changes in hydrology during the last glacial period. Data show low values during late MIS 3 and deglaciation (20–11 ka) and high values during the LGM (27–18 ka) (Fig. 5B). The extreme aridity in the three short periods (39–37 ka, 22–21 ka, and 13–11 ka) is inferred by the positive excursions, corresponding to the H4, H2, and YD, respectively. The H1 and H3 events are not as prominent as the YD, H2, and H4 events in the new isotopic record.

Strong Asian Summer Monsoons during Late MIS 3

New $\delta^2H_{n\text{-alk-T}}$ values and U^K_{37}-based lake temperatures co-vary with the summer insolation during the last glacial period. Low isotopic values and warm temperatures occur during the high summer isolation period, while high isotopic values and cold temperatures occur during the low summer insolation period (Figs. 5A–5C). Speleothem $\delta^{18}O$ records from the Dongge and Hulu Caves in East Asia show similar isotopic patterns with low precipitation $\delta^{18}O$ values corresponding to enhanced rainfall during high summer insolation and high $\delta^{18}O$ values corresponding to reduced rainfall during low summer insolation (Fig. 5E) (Dykoski et al., 2005; Wang et al., 2008). The intensity of the Asian summer monsoons is primarily controlled by land-ocean thermal contrast, latent heating over the Tibetan Plateau, and equatorial Pacific sea surface temperature at both the millennial and precessional scale (Webster et al., 1998; Molnar et al., 2010; Wu et al., 2012; Caley et al., 2014). Plant wax $\delta^2H_{n\text{-alk}}$ records (Thomas et al., 2016; Hou et al., 2017) and ostracod $\delta^{18}O$ records (Chen et al., 2016) from Lake Qinghai indicate that the Asian summer monsoons were strong during the early Holocene when summer insolation was high. Our new $\delta^2H_{n\text{-alk-T}}$ records from the drill core for late MIS 3 (30–45 ka), except for the H4 event (Fig. 5B), have similar isotopic values to that of Lake Keluke during the early Holocene (Rao et al., 2014). Given that the Qaidam Basin lies on the boundary between the Westerlies and the Asian summer monsoons, we argue that the strong Asian summer monsoons that are driven by precessional forcing penetrated further into Central Asia during the warm, late MIS 3, resulting in increased precipitation and lower $\delta^2H_{n\text{-alk-T}}$ values as demonstrated in the Qaidam core.

The isotopic records from Central Asia support our interpretation of enhanced northward penetration of Asian summer monsoon moisture associated with migration of the climatic boundary into the Asian interior during MIS 3. Speleothem $\delta^{18}O$ records from the Ton Cave and Kesang Cave near the present Westerlies area further west of our study area (Fig. 1) show the cyclic incursions of Asian summer monsoons into Central Asia since ca. 500 ka (Cheng et al., 2012). The leaf wax $\delta^2H_{n\text{-alk}}$ record from the Pamirs at the southwestern border of the Westerly-influenced region reveals a similar pattern during the early Holocene when summer insolation is high and the strong Asian summer monsoons penetrate deep into Central Asia (Aichner et al., 2019).

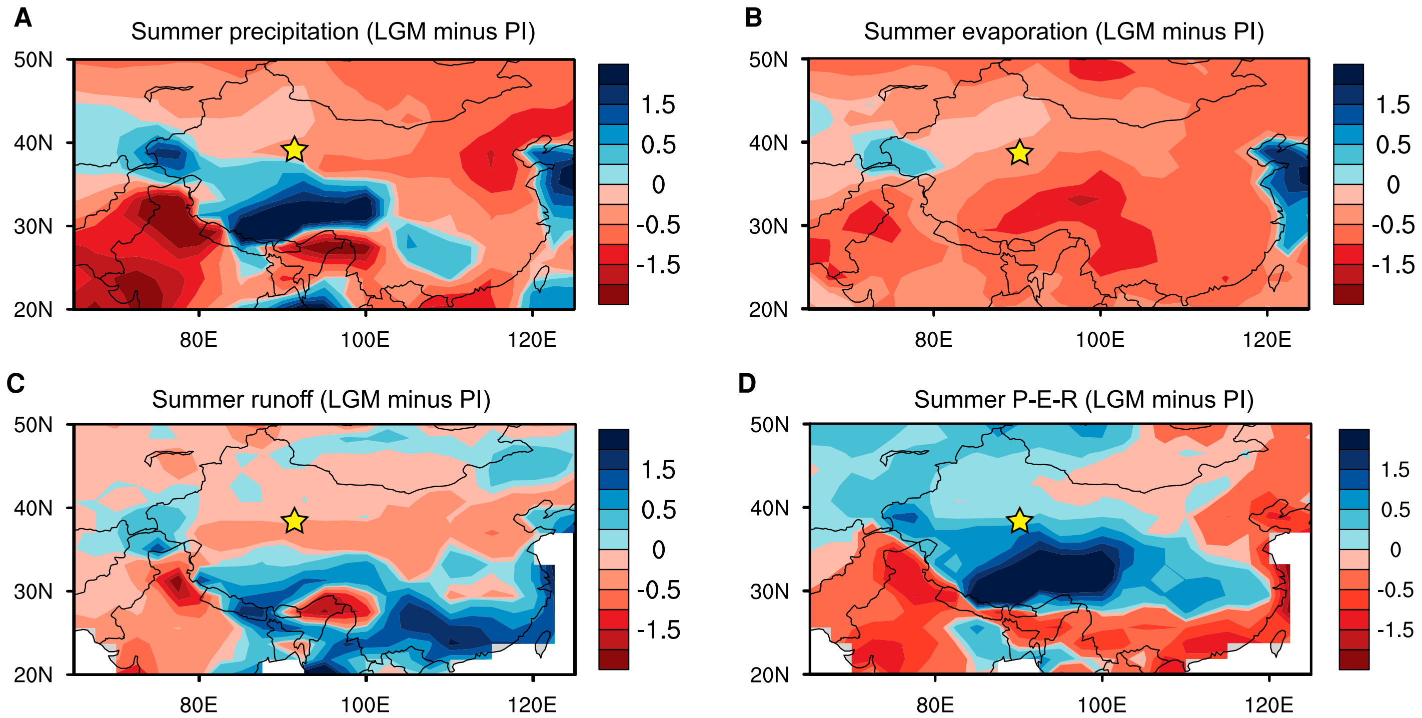

Figure 6. Numerical modeling results are plotted on Hovmoller diagrams for (A) precipitation, (B) evaporation, (C) runoff, and (D) effective precipitation (P_e; calculated from Equation 7) during summer. Model results for precipitation include both liquid (rain) and solid (snow). The yellow star indicates the Qaidam Basin. Units: mm/day. LGM—Last Glacial Maximum; PI—pre-industrial.

Low $\delta^2H_{n\text{-alk-T}}$ values are concurrent with peak P_{aq} ratios between 30 ka and 37 ka. (Fig. 5D). The high P_{aq} values could result from either an increase of aquatic macrophytes and/or a decrease of terrestrial plant input. Paleo-shoreline records from the Tibetan Plateau and adjacent desert regions show that the paleo lakes (Fig. 1) expanded at ~40–30 ka with lake levels 30–280 m higher than at present (Chen and Bowler, 1986; Zhang et al., 2008). Given that the terrestrial plants expanded during MIS 3 in the northern Tibetan Plateau (Herzschuh et al., 2006), we suggest that the variations in P_{aq} values reflect changes in local hydrological conditions that result in a substantial increase in the proportion of biomarkers produced by the aquatic plants relative to those produced by the terrestrial plants and preserved in the sediment core. High P_{aq} values at ca. 37–30 ka are likely to reflect a shift in the paleohydrological condition of the paleolake from shallow and proximal to a deep and distal lacustrine environment accompanied by enhanced lake production during the strong Asian summer monsoon period.

Previous results are interpreted to show that the wet climate during late MIS 3 in northwestern China is linked to increasing circulation of the Westerlies during the glacial period (Yang et al., 2004). The Westerlies' wind index of grain-size data from Tianshan and the Chinese Loess Plateau along the Westerlies route supports the argument that the Westerlies were stronger during MIS 3 than at present but weaker than during the LGM (Fig. 5F) (Sun et al., 2012; Rao et al., 2013; Li et al., 2016). However, in the Westerly-controlled Mediterranean region, lake levels during MIS 3 were lower than during the LGM due to the weaker storm track of the Westerlies (Bartov et al., 2003; Torfstein et al., 2013). Our low $\delta^2H_{n\text{-alk-T}}$ values suggest that the late MIS 3 was wetter than during the LGM, which differs from hydrologic patterns in the core area of the Westerly-influenced region. Hence, we infer that the warm, wet paleoclimate is associated with intensified Asian summer monsoons rather than with the Westerlies.

High Effective Precipitation and Reduced Evaporation during the LGM

$\delta^2H_{n\text{-alk-T}}$ values increase from the end of MIS 3 to the LGM (Fig. 5B). We interpret that increasing $\delta^2H_{n\text{-alk-T}}$ values indicate that the climate became drier as the Asian summer monsoons retreated from Central Asia when summer insolation declined. As a result, the Westerlies advanced and acted as the primary moisture source to the Qaidam Basin during the LGM. A southward extension of the ice sheet in the Northern Hemisphere during the LGM potentially enlarged the meridional thermal gradient and strengthened the mid-latitude Westerlies (COHMAP members, 1988; Toggweiler and Russell, 2008; Sun et al., 2012; Wang et al., 2018). Grain-size analysis and hydrologic reconstruction of lacustrine sediments from the northeastern Tibetan Plateau supports cold and dry climate being associated with the enhanced Westerlies during the LGM (An et al., 2012; Wang et al., 2014; Thomas et al., 2016). Pollen records also show an increase in cold-tolerant and arid-tolerant plants, represented by alpine desert and alpine sparse during the LGM in nearby Qilian Shan (Herzschuh et al., 2006).

During the LGM, $\delta^2H_{n\text{-alk-T}}$ values of the Qaidam core were lower than those of Lake Sugan (Fig. 5B), which implies a less arid climate. The $\delta^2H_{n\text{-alk-T}}$ values are comparable to those of Lake Keluke since the late Holocene, indicating that LGM hydrological conditions in Western Qaidam were similar to those in the eastern part at present. Our climate simulations of the LGM show that summer precipitation decreases in the western Qaidam Basin by 0.25–0.5 mm/day more than during the PI (Fig. 6A). The modeled evaporation is also reduced during the LGM relative to that of the PI, likely resulting from low temperatures due to minimal summer insolation (Fig. 6B) (Allen et al., 1998). The runoff also declines during the LGM, reflecting a reduction in soil water infiltration and recharge (Fig. 6C). The reduction in evaporation and runoff surpasses that of precipitation, leading to an increase in effective precipitation (P_e) during the LGM relative to that of the PI (Fig. 6D). Recent isotope proxy data and climate simulation results from the Pamirs also highlight the importance of decreased summer evaporation in triggering lake transgression during the last glacial period (Aichner et al., 2019). The climate simulation results support our interpretation of $\delta^2H_{n\text{-alk-T}}$ records for an overall cold, arid climate during the LGM that was wetter than at present.

Short-Period Aridity During Extreme Cold Events

Three pronounced positive $\delta^2H_{n\text{-alk}}$ excursions and cold U_{37}^{K} temperatures during the YD, H2, and H4 events indicate millennial-scale pulses of aridity (Fig. 5). Proxy records and climate models suggest that freshwater discharge from the Laurentide ice sheet during the Heinrich stadials slowed down the Atlantic meridional overturning circulation and reduced the northward oceanic heat transport, which cooled the Northern Hemisphere (Bond et al., 1997; Kageyama et al., 2010; Sun et al., 2012; Henry et al., 2016). The change in Atlantic circulation drove the short period of aridity in both the Westerly and monsoon areas. For example, the shoreline record of paleolake Lisan in the eastern Mediterranean region shows that the general high lake level during the LGM was interrupted by drought phases during the Heinrich events, which resulted from a brief shutdown of Mediterranean storm activity due to the cooler ocean temperature (Bartov et al., 2003; Torfstein et al., 2013). Pollen records from the Yili Basin in Central Asia suggest that an arid climate during the Younger Dryas was associated with cooling of the North Atlantic sea surface temperature (Li et al., 2011b). In East Asia, climate models indicate that cooling in the North Atlantic shifts the intertropical convergence zone southward and weakens the summer monsoons (Zhang and Delworth, 2005; Sun et al., 2012), which is in agreement with the speleothem and loess/paleosol records (Dykoski et al., 2005; Wang et al., 2008; Rao et al., 2013).

CONCLUSIONS

New biomarker and isotope proxy studies show that the paleohydrology and lake temperatures of the Qaidam Basin varied in response to precessional forcing during 45–11 ka. A new $\delta^2H_{n\text{-alk-T}}$ record shares similar characteristics with the isotopic signatures from Asian summer monsoon-influenced regions: the lower $\delta^2H_{n\text{-alk-T}}$ values and enhanced precipitation occurred during high summer insolation. We suggest that the enhanced northward penetration of Asian summer monsoon moisture produced a wetter climate during the late MIS 3 (45–39 ka and 37–33 ka) with the climate boundary between the Westerlies and the Asian summer monsoons penetrating further into Central Asia under high summer insolation. A cold, arid climate dominated the region during the LGM, when the Asian summer monsoons retreated, but with a substantial reduction in evaporation and surface runoff. We ascribe this to the unique location of the Qaidam Basin that links the Westerlies and Asian summer monsoons in the Northern Hemisphere. The two atmospheric systems alternately control the climate in the Qaidam Basin as a result of their relative strength. Extreme aridity is induced by the interruption of moisture transport from the Westerlies and Asian summer monsoons during the North Atlantic events. New isotopic and temperature data support the cold, dry climate in glacial/stadial periods and warm, wet climate in interglacial/interstadial periods. These new results provide evidence that the paleo-lake may have expanded during the LGM due in large part to the effect of reduced evaporation.

ACKNOWLEDGMENTS

We thank Associate Editor Ganqing Jiang and reviewers Alex Pullen and Lin Li for thorough and constructive comments that significantly improved the quality of the paper. We thank the drilling team and the China University of Geosciences, Wuhan, for providing the core samples. We also thank Jiang Zhu of the National Center for Atmospheric Research for providing simulations and helpful discussions on the model configurations, Yongbo Peng for assistance in laboratory work, and Linlin Cui for help with Figure 1. This work is supported by a National Science Foundation grant (award #2022282) to G. Zhuang.

REFERENCES CITED

Aichner, B., Makhmudov, Z., Rajabov, I., Zhang, Q., Pausata, F.S.R., Werner, M., Heinecke, L., Kuessner, M.L., Feakins, S.J., Sachse, D., and Mischke, S., 2019, Hydroclimate in the Pamirs was driven by changes in precipitation-evaporation seasonality since the Last Glacial Period: Geophysical Research Letters, v. 46, no. 23, p. 13972–13983, https://doi.org/10.1029/2019GL085202.

Allen, R.G., Pereira, L.S., Raes, D., and Smith, M., 1998, Crop Evapotranspiration—Guidelines for Computing Crop Water Requirements—FAO Irrigation and Drainage Paper 56: Rome, Fao, v. 300, no. 9, D05109.

Alley, R.B., 2000, The Younger Dryas cold interval as viewed from central Greenland: Quaternary Science Reviews, v. 19, no. 1–5, p. 213–226, https://doi.org/10.1016/S0277-3791(99)00062-1.

An, Z., Liu, T., Lu, Y., Porter, S., Kukla, G., Wu, X., and Hua, Y., 1990, The long-term paleomonsoon variation recorded by the loess-paleosol sequence in central China: Quaternary International, v. 7, p. 91–95.

An, Z., Colman, S.M., Zhou, W., Li, X., Brown, E.T., Jull, A.J.T., Cai, Y., Huang, Y., Lu, X., Chang, H., Song, Y., Sun, Y., Xu, H., Liu, W., Jin, Z., Liu, X., Cheng, P., Liu, Y., Ai, L., Li, X., Liu, X., Yan, L., Shi, Z., Wang, X., Wu, F., Qiang, X., Dong, J., Lu, F., and Xu, X., 2012, Interplay between the Westerlies and Asian monsoon recorded in Lake Qinghai sediments since 32 ka: Scientific Reports, v. 2, https://doi.org/10.1038/srep00619.

Araguás-Araguás, L., Froehlich, K., and Rozanski, K., 1998, Stable isotope composition of precipitation over southeast Asia: Journal of Geophysical Research: Atmospheres, v. 103, no. D22, p. 28721–28742, https://doi.org/10.1029/98JD02582.

Bartov, Y., Goldstein, S.L., Stein, M., and Enzel, Y., 2003, Catastrophic arid episodes in the Eastern Mediterranean linked with the North Atlantic Heinrich events: Geology, v. 31, no. 5, p. 439–442, https://doi.org/10.1130/0091-7613(2003)031<0439:CAEITE>2.0.CO;2.

Berger, A., 1978, Long-term variations of caloric insolation resulting from the Earth's orbital elements: Quaternary Research, v. 9, no. 2, p. 139–167, https://doi.org/10.1016/0033-5894(78)90064-9.

Bershaw, J., Penny, S.M., and Garzione, C.N., 2012, Stable isotopes of modern water across the Himalaya and eastern Tibetan Plateau: Implications for estimates of paleoelevation and paleoclimate: Journal of Geophysical Research: Atmospheres, v. 117, https://doi.org/10.1029/2011JD016132.

Bond, G., Showers, W., Cheseby, M., Lotti, R., Almasi, P., DeMenocal, P., Priore, P., Cullen, H., Hajdas, I., and Bonani, G., 1997, A pervasive millennial-scale cycle in North Atlantic Holocene and glacial climates: Science, v. 278, no. 5341, p. 1257–1266, https://doi.org/10.1126/science.278.5341.1257.

Brassell, S., Eglinton, G., Marlowe, I., Pflaumann, U., and Sarnthein, M., 1986, Molecular stratigraphy: A new tool for climatic assessment: Nature, v. 320, no. 6058, p. 129–133, https://doi.org/10.1038/320129a0.

Caley, T., Roche, D.M., and Renssen, H., 2014, Orbital Asian summer monsoon dynamics revealed using an isotope-enabled global climate model: Nature Communications, v. 5, no. 5371, https://doi.org/10.1038/ncomms6371.

Caves, J.K., Winnick, M.J., Graham, S.A., Sjostrom, D.J., Mulch, A., and Chamberlain, C.P., 2015, Role of the westerlies in Central Asia climate over the Cenozoic: Earth and Planetary Science Letters, v. 428, p. 33–43, https://doi.org/10.1016/j.epsl.2015.07.023.

Chen, F., Wu, D., Chen, J., Zhou, A., Yu, J., Shen, J., Wang, S., and Huang, X., 2016, Holocene moisture and East Asian summer monsoon evolution in the northeastern Tibetan Plateau recorded by Lake Qinghai and its environs: A review of conflicting proxies: Quaternary Science Reviews, v. 154, p. 111–129, https://doi.org/10.1016/j.quascirev.2016.10.021.

Chen, K., and Bowler, J., 1986, Late Pleistocene evolution of salt lakes in the Qaidam basin, Qinghai province, China: Palaeogeography, Palaeoclimatology, Palaeoecology, v. 54, no. 1–4, p. 87–104.

Cheng, H., Zhang, P.Z., Spötl, C., Edwards, R.L., Cai, Y.J., Zhang, D.Z., Sang, W.C., Tan, M., and An, Z.S., 2012, The climatic cyclicity in semiarid-arid central Asia over the past 500,000 years: Geophysical Research Letters, v. 39, no. 1, https://doi.org/10.1029/2011GL050202.

Cheng, H., Spoetl, C., Breitenbach, S.F.M., Sinha, A., Wassenburg, J.A., Jochum, K.P., Scholz, D., Li, X., Yi, L., Peng, Y., Lv, Y., Zhang, P., Votintseva, A., Loginov, V., Ning, Y., Kathayat, G., and Edwards, R.L., 2016, Climate variations of Central Asia on orbital to millennial timescales: Scientific Reports, v. 6, https://doi.org/10.1038/srep36975.

Clark, P.U., Dyke, A.S., Shakun, J.D., Carlson, A.E., Clark, J., Wohlfarth, B., Mitrovica, J.X., Hostetler, S.W., and McCabe, A.M., 2009, The Last Glacial Maximum: Science, v. 325, no. 5941, p. 710–714, https://doi.org/10.1126/science.1172873.

COHMAP members, 1988, Climatic changes of the last 18,000 years: Observations and model simulations: Science, v. 241, p. 1043–1052.

Dykoski, C., Edwards, R., Cheng, H., Yuan, D., Cai, Y., Zhang, M., Lin, Y., Qing, J., An, Z., and Revenaugh, J., 2005, A high-resolution, absolute-dated Holocene and deglacial Asian monsoon record from Dongge Cave, China: Earth and Planetary Science Letters, v. 233, no. 1–2, p. 71–86, https://doi.org/10.1016/j.epsl.2005.01.036.

Eglinton, G., and Hamilton, R.J., 1967, Leaf epicuticular waxes: Science, v. 156, no. 3780, p. 1322, https://doi.org/10.1126/science.156.3780.1322.

Ficken, K.J., Li, B., Swain, D., and Eglinton, G., 2000, An n-alkane proxy for the sedimentary input of submerged/floating freshwater aquatic macrophytes: Organic Geochemistry, v. 31, no. 7, p. 745–749, https://doi.org/10.1016/S0146-6380(00)00081-4.

Goudie, A.S., 2007, Mega-yardangs: A global analysis: Geography Compass, v. 1, no. 1, p. 65–81, https://doi.org/10.1111/j.1749-8198.2006.00003.x.

He, Y., Liu, W., Zhao, C., Wang, Z., Wang, H., Liu, Y., Qin, X., Hu, Q., An, Z., and Liu, Z., 2013, Solar influenced late Holocene temperature changes on the northern Tibetan Plateau: Chinese Science Bulletin, v. 58, no. 9, p. 1053–1059, https://doi.org/10.1007/s11434-012-5619-8.

Heermance, R.V., Pullen, A., Kapp, P., Garzione, C.N., Bogue, S., Ding, L., and Song, P., 2013, Climatic and tectonic controls on sedimentation and erosion during the Pliocene–Quaternary in the Qaidam Basin (China): Geological Society of America Bulletin, v. 125, no. 5–6, p. 833–856, https://doi.org/10.1130/B30748.1.

Hemming, S.R., 2004, Heinrich events: Massive late Pleistocene detritus layers of the North Atlantic and their global climate imprint: Reviews of Geophysics, v. 42, no. 1, https://doi.org/10.1029/2003RG000128.

Hendy, C.H., and Hall, B.L., 2006, The radiocarbon reservoir effect in proglacial lakes: Examples from Antarctica: Earth and Planetary Science Letters, v. 241, no. 3–4, p. 413–421, https://doi.org/10.1016/j.epsl.2005.11.045.

Henry, L.G., McManus, J.F., Curry, W.B., Roberts, N.L., Piotrowski, A.M., and Keigwin, L.D., 2016, North Atlantic ocean circulation and abrupt climate change during the last glaciation: Science, v. 353, no. 6298, p. 470, https://doi.org/10.1126/science.aaf5529.

Herzschuh, U., Kürschner, H., and Mischke, S., 2006, Temperature variability and vertical vegetation belt shifts during the last ~50,000 yr in the Qilian Mountains (NE margin of the Tibetan Plateau, China): Quaternary Research, v. 66, no. 1, p. 133–146, https://doi.org/10.1016/j.yqres.2006.03.001.

Hou, J., D'Andrea, W.J., and Liu, Z., 2012, The influence of ^{14}C reservoir age on interpretation of paleolimnological records from the Tibetan Plateau: Quaternary Science Reviews, v. 48, p. 67–79, https://doi.org/10.1016/j.quascirev.2012.06.008.

Hou, J., Huang, Y., Zhao, J., Liu, Z., Colman, S., and An, Z., 2016, Large Holocene summer temperature oscillations and impact on the peopling of the northeastern Tibetan Plateau: Geophysical Research Letters, v. 43, no. 3, p. 1323–1330, https://doi.org/10.1002/2015GL067317.

Hou, J., D'Andrea, W.J., Wang, M., He, Y., and Liang, J., 2017, Influence of the Indian monsoon and the subtropical jet on climate change on the Tibetan Plateau since the late Pleistocene: Quaternary Science Reviews, v. 163, p. 84–94, https://doi.org/10.1016/j.quascirev.2017.03.013.

Hovan, S., Rea, D.K., and Pisias, N.G., 1991, Late Pleistocene continental climate and oceanic variability recorded in northwest Pacific sediments: Paleoceanography and Paleoclimatology, v. 6, no. 3, p. 349–370, https://doi.org/10.1029/91PA00559.

IAEA/WMO, 2006, Global network of isotopes in precipitation: The GNIP database. Accessible at: http://isohis.iaea.org.

Kageyama, M., Paul, A., Roche, D.M., and Van Meerbeeck, C.J., 2010, Modelling glacial climatic millennial-scale variability related to changes in the Atlantic meridional overturning circulation: A review: Quaternary Science Reviews, v. 29, no. 21–22, p. 2931–2956, https://doi.org/10.1016/j.quascirev.2010.05.029.

Kageyama, M., Albani, S., Braconnot, P., Harrison, S.P., Hopcroft, P.O., Ivanovic, R.F., Lambert, F., Marti, O., Peltier, W.R., and Peterschmitt, J.Y., 2017, The PMIP4 contribution to CMIP6-Part 4: Scientific objectives and experimental design of the PMIP4-CMIP6 Last Glacial Maximum experiments and PMIP4 sensitivity experiments: Geoscientific Model Development, v. 10, no. 11, p. 4035–4055, https://doi.org/10.5194/gmd-10-4035-2017.

Kapp, P., Pelletier, J.D., Rohrmann, A., Heermance, R., Russell, J., and Ding, L., 2011, Wind erosion in the Qaidam basin, central Asia: Implications for tectonics, paleoclimate, and the source of the Loess Plateau: GSA Today, v. 21, no. 4/5, p. 4–10, https://doi.org/10.1130/GSATG99A.1.

Kukla, G., and An, Z., 1989, Loess stratigraphy in central China: Palaeogeography, Palaeoclimatology, Palaeoecology, v. 72, p. 203–225, https://doi.org/10.1016/0031-0182(89)90143-0.

Li, B., and Zhu, L., 2001, "Greatest lake period" and its palaeo-environment on the Tibetan Plateau: Journal of Geographical Sciences, v. 11, no. 1, p. 34–42, https://doi.org/10.1007/BF02837374.

Li, G., Pettke, T., and Chen, J., 2011a, Increasing Nd isotopic ratio of Asian dust indicates progressive uplift of the north Tibetan Plateau since the middle Miocene: Geology, v. 39, no. 3, p. 199–202, https://doi.org/10.1130/G31734.1.

Li, G., Rao, Z., Duan, Y., Xia, D., Wang, L., Madsen, D.B., Jia, J., Wei, H., Qiang, M., Chen, J., and Chen, F., 2016, Paleoenvironmental changes recorded in a luminescence dated loess/paleosol sequence from the Tianshan Mountains, arid central Asia, since the Penultimate Glaciation: Earth and Planetary Science Letters, v. 448, p. 1–12, https://doi.org/10.1016/j.epsl.2016.05.008.

Li, L., and Garzione, C.N., 2017, Spatial distribution and controlling factors of stable isotopes in meteoric waters on the Tibetan Plateau: Implications for paleoelevation reconstruction: Earth and Planetary Science Letters, v. 460, p. 302–314, https://doi.org/10.1016/j.epsl.2016.11.046.

Li, L., Fan, M., Davila, N., Jesmok, G., Mitsunaga, B., Tripati, A., and Orme, D., 2019, Carbonate stable and clumped isotopic evidence for late Eocene moderate to high elevation of the east-central Tibetan Plateau and its geodynamic implications: Geological Society of America Bulletin, v. 131, p. 831–844, https://doi.org/10.1130/B32060.1.

Li, X., Zhao, K., Dodson, J., and Zhou, X., 2011b, Moisture dynamics in central Asia for the last 15 kyr: New evidence from Yili Valley, Xinjiang, NW China: Quaternary Science Reviews, v. 30, no. 23–24, p. 3457–3466, https://doi.org/10.1016/j.quascirev.2011.09.010.

Lin, X., Chang, H., Wang, K., Zhang, G., and Meng, G., 2020, Machine learning for source identification of dust on the Chinese Loess Plateau: Geophysical Research Letters, https://doi.org/10.1029/2020GL088950.

Mix, A.C., Bard, E., and Schneider, R., 2001, Environmental processes of the ice age: Land, oceans, glaciers (EPILOG): Quaternary Science Reviews, v. 20, no. 4, p. 627–657, https://doi.org/10.1016/S0277-3791(00)00145-1.

Molnar, P., Boos, W.R., and Battisti, D.S., 2010, Orographic controls on climate and paleoclimate of Asia: Thermal and mechanical roles for the Tibetan Plateau: Annual Review of Earth and Planetary Sciences, v. 38, p. 77–102, https://doi.org/10.1146/annurev-earth-040809-152456.

Oleson, K.W., Lawrence, D.M., Gordon, B., Flanner, M.G., Kluzek, E., Peter, J., Levis, S., Swenson, S.C., Thornton, E., and Feddema, J., 2010, Technical description of version 4.0 of the Community Land Model (CLM): University Corporation for Atmospheric Research, https://doi.org/10.5065/D6FB50WZ.

Peltier, W.R., Argus, D.F., and Drummond, R., 2015, Space geodesy constrains ice age terminal deglaciation: The global ICE-6G_C (VM5a) model: Journal of Geophysical Research: Solid Earth, v. 120, no. 1, p. 450–487, https://doi.org/10.1002/2014JB011176.

Polissar, P.J., Freeman, K.H., Rowley, D.B., McInerney, F.A., and Currie, B.S., 2009, Paleoaltimetry of the Tibetan Plateau from D/H ratios of lipid biomarkers: Earth and Planetary Science Letters, v. 287, no. 1–2, p. 64–76, https://doi.org/10.1016/j.epsl.2009.07.037.

Porter, S.C., and An, Z., 1995, Correlation between climate events in the North Atlantic and China during the last glaciation: Nature, v. 375, no. 6529, p. 305, https://doi.org/10.1038/375305a0.

Prahl, F.G., and Wakeham, S.G., 1987, Calibration of unsaturation patterns in long-chain ketone compositions for palaeotemperature assessment: Nature, v. 330, no. 6146, p. 367, https://doi.org/10.1038/330367a0.

Pullen, A., Kapp, P., McCallister, A.T., Chang, H., Gehrels, G.E., Garzione, C.N., Heermance, R.V., and Ding, L., 2011, Qaidam Basin and northern Tibetan Plateau as dust sources for the Chinese Loess Plateau and paleoclimatic implications: Geology, v. 39, no. 11, p. 1031–1034, https://doi.org/10.1130/G32296.1.

Rao, Z., Chen, F., Cheng, H., Liu, W., Wang, G., Lai, Z., and Bloemendal, J., 2013, High-resolution summer precipitation variations in the western Chinese Loess Plateau during the last glacial: Scientific Reports, v. 3, no. 2785, https://doi.org/10.1038/srep02785.

Rao, Z., Jia, G., Qiang, M., and Zhao, Y., 2014, Assessment of the difference between mid- and long chain compound specific δDn-alkanes values in lacustrine sediments as a paleoclimatic indicator: Organic Geochemistry, v. 76, p. 104–117, https://doi.org/10.1016/j.orggeochem.2014.07.015.

Rohrmann, A., Heermance, R., Kapp, P., and Cai, F., 2013, Wind as the primary driver of erosion in the Qaidam Basin, China: Earth and Planetary Science Letters, v. 374, p. 1–10, https://doi.org/10.1016/j.epsl.2013.03.011.

Sachse, D., Billault, I., Bowen, G.J., Chikaraishi, Y., Dawson, T.E., Feakins, S.J., Freeman, K.H., Magill, C.R., McInerney, F.A., van der Meer, M.T.J., Polissar, P., Robins, R.J., Sachs, J.P., Schmidt, H.-L., Sessions, A.L., White, J.W.C., West, J.B., and Kahmen, A., 2012, Molecular paleohydrology: Interpreting the hydrogen-isotopic composition of lipid biomarkers from photosynthesizing organisms: Annual Review of Earth and Planetary Sciences, v. 40, no. 1, p. 221–249, https://doi.org/10.1146/annurev-earth-042711-105535.

Schouten, S., Hopmans, E.C., Schefuss, E., and Damste, J.S.S., 2002, Distributional variations in marine crenarchaeotal membrane lipids: A new tool for reconstructing ancient sea water temperatures?: Earth and Planetary Science Letters, v. 204, no. 1–2, p. 265–274, https://doi.org/10.1016/S0012-821X(02)00979-2.

Shakun, J.D., Clark, P.U., He, F., Marcott, S.A., Mix, A.C., Liu, Z., Otto-Bliesner, B., Schmittner, A., and Bard, E., 2012, Global warming preceded by increasing carbon dioxide concentrations during the last deglaciation: Nature, v. 484, no. 7392, p. 49–54, https://doi.org/10.1038/nature10915.

Shi, Y., Yu, G., Liu, X., Li, B., and Yao, T., 2001, Reconstruction of the 30–40 ka BP enhanced Indian monsoon climate based on geological records from the Tibetan Plateau: Palaeogeography, Palaeoclimatology, Palaeoecology, v. 169, no. 1, p. 69–83, https://doi.org/10.1016/S0031-0182(01)00216-4.

Sun, Y., Clemens, S.C., Morrill, C., Lin, X., Wang, X., and An, Z., 2012, Influence of Atlantic meridional overturning circulation on the East Asian winter monsoon: Nature Geoscience, v. 5, no. 1, p. 46, https://doi.org/10.1038/ngeo1326.

Thomas, E.K., Huang, Y., Clemens, S.C., Colman, S.M., Morrill, C., Wegener, P., and Zhao, J., 2016, Changes in dominant moisture sources and the consequences for hydroclimate on the northeastern Tibetan Plateau during the past 32 kyr: Quaternary Science Reviews, v. 131, p. 157–167, https://doi.org/10.1016/j.quascirev.2015.11.003.

Thompson, L.G., Mosley-Thompson, E., Davis, M., Bolzan, J., Dai, J., Yao, T., Gundestrup, N., Wu, X., Klein, L., and Xie, Z., 1989, Holocene-late Pleistocene climatic ice core records from Qinghai-Tibetan Plateau: Science, v. 246, no. 4929, p. 474–477, https://doi.org/10.1126/science.246.4929.474.

Thompson, L.G., Yao, T., Davis, M.E., Henderson, K.A., Mosley-Thompson, E., Lin, P.N., Beer, J., Synal, H.A., Cole-Dai, J., and Bolzan, J.F., 1997, Tropical climate instability: The last glacial cycle from a Qinghai-Tibetan ice core: Science, v. 276, no. 5320, p. 1821–1825, https://doi.org/10.1126/science.276.5320.1821.

Tian, L., Masson-Delmotte, V., Stievenard, M., Yao, T., and Jouzel, J., 2001, Tibetan Plateau summer monsoon northward extent revealed by measurements of water stable isotopes: Journal of Geophysical Research: Atmospheres, v. 106, no. D22, p. 28081–28088, https://doi.org/10.1029/2001JD900186.

Tian, L., Yao, T., Schuster, P.F., White, J.W.C., Ichiyanagi, K., Pendall, E., Pu, J., and Wu, Y., 2003, Oxygen-18 concentrations in recent precipitation and ice cores on the Tibetan Plateau: Journal of Geophysical

Research: Atmospheres, v. 108, no. D9, https://doi.org/10.1029/2002JD002173.

Tierney, J., Zhu, J., King, J., Malevich, S.B., Hakim, G., and Poulsen, C., 2020, Glacial cooling and climate sensitivity revisited: Nature, v. 584, p. 569–573, https://doi.org/10.1038/s41586-020-2617-x.

Toggweiler, J.R., and Russell, J., 2008, Ocean circulation in a warming climate: Nature, v. 451, no. 7176, p. 286–288, https://doi.org/10.1038/nature06590.

Torfstein, A., Goldstein, S.L., Stein, M., and Enzel, Y., 2013, Impacts of abrupt climate changes in the Levant from Last Glacial Dead Sea levels: Quaternary Science Reviews, v. 69, p. 1–7, https://doi.org/10.1016/j.quascirev.2013.02.015.

Wang, N., Jiang, D., and Lang, X., 2018, Northern Westerlies during the Last Glacial Maximum: Results from CMIP5 Simulations: Journal of Climate, v. 31, no. 3, p. 1135–1153, https://doi.org/10.1175/JCLI-D-17-0314.1.

Wang, Y., Cheng, H., Edwards, R.L., Kong, X., Shao, X., Chen, S., Wu, J., Jiang, X., Wang, X., and An, Z., 2008, Millennial- and orbital-scale changes in the East Asian monsoon over the past 224,000 years: Nature, v. 451, no. 7182, p. 1090, https://doi.org/10.1038/nature06692.

Wang, Y., Herzschuh, U., Shumilovskikh, L.S., Mischke, S., Birks, H.J.B., Wischnewski, J., Böhner, J., Schlütz, F., Lehmkuhl, F., Diekmann, B., Wünnemann, B., and Zhang, C., 2014, Quantitative reconstruction of precipitation changes on the NE Tibetan Plateau since the Last Glacial Maximum—Extending the concept of pollen source area to pollen-based climate reconstructions from large lakes: Climate of the Past, v. 10, no. 1, p. 21–39, https://doi.org/10.5194/cp-10-21-2014.

Wang, Z., and Liu, W., 2013, Calibration of the U^{K}_{37} index of long-chain alkenones with the in-situ water temperature in Lake Qinghai in the Tibetan Plateau: Chinese Science Bulletin, v. 58, no. 7, p. 803–808, https://doi.org/10.1007/s11434-012-5527-y.

Wang, Z., Liu, W., Liu, Z., Wang, H., He, Y., and Zhang, F., 2013, A 1700-year n-alkanes hydrogen isotope record of moisture changes in sediments from Lake Sugan in the Qaidam Basin, northeastern Tibetan Plateau: The Holocene, v. 23, no. 9, p. 1350–1354, https://doi.org/10.1177/0959683613486941.

Webster, P.J., Magana, V.O., Palmer, T., Shukla, J., Tomas, R., Yanai, M., and Yasunari, T., 1998, Monsoons: Processes, predictability, and the prospects for prediction: Journal of Geophysical Research: Oceans, v. 103, no. C7, p. 14451–14510, https://doi.org/10.1029/97JC02719.

Wu, G., Liu, Y., He, B., Bao, Q., Duan, A., and Jin, F.-F., 2012, Thermal controls on the Asian summer monsoon: Scientific Reports, v. 2, p. 404, https://doi.org/10.1038/srep00404.

Yang, B., Shi, Y., Braeuning, A., and Wang, J., 2004, Evidence for a warm-humid climate in arid northwestern China during 40–30 ka BP: Quaternary Science Reviews, v. 23, no. 23–24, p. 2537–2548, https://doi.org/10.1016/j.quascirev.2004.06.010.

Yao, T., Thompson, L., Yang, W., Yu, W., Gao, Y., Guo, X., Yang, X., Duan, K., Zhao, H., Xu, B., Pu, J., Lu, A., Xiang, Y., Kattel, D.B., and Joswiak, D., 2012, Different glacier status with atmospheric circulations in Tibetan Plateau and surroundings: Nature Climate Change, v. 2, no. 9, p. 663–667, https://doi.org/10.1038/nclimate1580.

Yao, T., Masson-Delmotte, V., Gao, J., Yu, W., Yang, X., Risi, C., Sturm, C., Werner, M., Zhao, H., and He, Y., 2013, A review of climatic controls on $\delta^{18}O$ in precipitation over the Tibetan Plateau: Observations and simulations: Reviews of Geophysics, v. 51, no. 4, p. 525–548, https://doi.org/10.1002/rog.20023.

Yu, G., Xue, B., Liu, J., and Chen, X., 2003, LGM lake records from China and an analysis of climate dynamics using a modelling approach: Global and Planetary Change, v. 38, no. 3–4, p. 223–256, https://doi.org/10.1016/S0921-8181(02)00257-6.

Zhang, H.-C., Fan, H., Chang, F.-Q., Zhang, W.-X., Lei, G., Yang, M., Lei, Y., and Yang, L., 2008, AMS dating on the shell bar section from Qaidam Basin, NE Tibetan Plateau, China: Radiocarbon, v. 50, no. 2, p. 255–265, https://doi.org/10.1017/S0033822200033555.

Zhang, R., and Delworth, T.L., 2005, Simulated tropical response to a substantial weakening of the Atlantic thermohaline circulation: Journal of Climate, v. 18, no. 12, p. 1853–1860, https://doi.org/10.1175/JCLI3460.1.

Zhang, X., Xu, B., Günther, F., Mügler, I., Lange, M., Zhao, H., Li, J., and Gleixner, G., 2017, Hydrogen isotope ratios of terrestrial leaf wax n-alkanes from the Tibetan Plateau: Controls on apparent enrichment factors, effect of vapor sources and implication for altimetry: Geochimica et Cosmochimica Acta, v. 211, p. 10–27, https://doi.org/10.1016/j.gca.2017.04.035.

Zhou, A., Chen, F., Qiang, M., Yang, M., and Zhang, J., 2007, The discovery of annually laminated sediments (varves) from shallow Sugan Lake in inland arid China and their paleoclimatic significance: Science in China Series D: Earth Sciences, v. 50, no. 8, p. 1218–1224, https://doi.org/10.1007/s11430-007-0081-1.

Zhou, A.-f., Chen, F.-h., Wang, Z.-l., Yang, M.-l., Qiang, M.-r., and Zhang, J.-w., 2009, Temporal Change of Radiocarbon Reservoir Effect in Sugan Lake, Northwest China during the Late Holocene: Radiocarbon, v. 51, no. 2, p. 529–535, https://doi.org/10.1017/S0033822200055909.

Zhu, J., Liu, Z., Brady, E., Otto-Bliesner, B., Zhang, J., Noone, D., Tomas, R., Nusbaumer, J., Wong, T., Jahn, A., and Tabor, C., 2017, Reduced ENSO variability at the LGM revealed by an isotope-enabled Earth system model: Geophysical Research Letters, v. 44, no. 13, p. 6984–6992, https://doi.org/10.1002/2017GL073406.

Zhuang, G., Brandon, M.T., Pagani, M., and Krishnan, S., 2014, Leaf wax stable isotopes from Northern Tibetan Plateau: Implications for uplift and climate since 15 Ma: Earth and Planetary Science Letters, v. 390, p. 186–198, https://doi.org/10.1016/j.epsl.2014.01.003.

Science Editor: Brad. S. Singer
Associate Editor: Ganqing Jiang

Manuscript Received 11 May 2020
Revised Manuscript Received 18 September 2020
Manuscript Accepted 1 October 2020

Printed in the USA